IFAC Journal of Systems and Control 11 (2020) 100074

Contents lists available at ScienceDirect

IFAC Journal of Systems and Control

journal homepage: www.elsevier.com/locate/ifacsc

Image-based feedback control for drift compensation in an electron microscope☆

E.P. van Horssen [a,*], B.J. Janssen [b], A. Kumar [a], D. Antunes [a], W.P.M.H. Heemels [a]

[a] Control Systems Technology Group, Eindhoven University of Technology, P.O. Box 513, 5600 MB Eindhoven, The Netherlands
[b] Thermo Fisher Scientific, Achtseweg Noord 5, 5651 GG Eindhoven, The Netherlands

ARTICLE INFO

Article history:
Received 10 November 2017
Received in revised form 8 December 2019
Accepted 17 January 2020
Available online 31 January 2020

Keywords:
Electron microscope
Image processing
Feature tracking
Delay
Feedback control
LQG
Switched systems

ABSTRACT

Electron microscopes are high-precision imaging systems that are used to image objects (specimens) up to atomic resolutions. Even in highly-controlled industrial sites with minimal external disturbances, internal disturbances cause the objects to move in the field of view of the imaging system. These internal disturbances are jointly considered as *drift*, which can prohibit fast and accurate imaging. The objective of this paper is to design a model-based control system that leads to the stabilization of the region of interest of the object in the center of the field of view despite the presence of drift, which can be achieved by controlling the movement of the object itself using an actuated positioning system (stage). An interesting feature of the problem is that the displacement of the object can only be measured through the imaging system itself, which requires a non-trivial image-processing step affected by significant delay and inaccuracy. In the image-processing step, a tracking algorithm provides drift estimates. The image-processing characteristics inherent to the tracking algorithm such as image-acquisition time, tracking delay, and measurement accuracy, are explicitly taken into account in a novel LQG-type control design for this application. The decision for a LQG-type control design is based on a stochastic model proposed for the drift motion of the specimen to include the uncertainty in the drift. Moreover, we show that new switched control designs can improve our original (non-switched) LQG design even further. To validate this approach, a simulator has been developed in close collaboration with an industrial OEM of electron microscopes to simulate a relevant industrial case study including tracking software and system parameters used in the industry. The simulator automatically generates and analyzes representative images to simulate closed-loop imaging and processing for feedback control.

1. Introduction

1.1. General problem setting and context

An electron microscope (EM) (Egerton, 2005; FEI, 2010) is a high-resolution tool for imaging objects (the specimens) at sub-Ångström resolutions (less than 0.1 nanometer per pixel, i.e., more than a million times more precise than the human eye). This makes EMs one of the primary tools for nanotechnology and other applications in life sciences, electronics manufacturing, and material sciences. By interaction of an electron beam with the specimen, the image is projected on a camera or a detector using magnetic lens systems, see, e.g., Fig. 1 for a schematic of a transmission electron microscope (TEM) (FEI, 2010; Reimer & Kohl, 2008). The image-acquisition process takes time, because a sufficient amount of electrons needs to be detected in order to provide enough contrast in an image, which is the main measure for image quality. In practice, high-quality images are obtained by averaging sequences of lower-quality images, which are obtained at intervals in the order of hundreds of milliseconds.

While nowadays EMs are mostly used as analysis tools in laboratories, their use in manufacturing industries is increasing. Industrial users of EMs usually wish to perform multiple imaging sessions for product analysis on various (batches of) specimens and therefore throughput becomes important. The throughput of specimens is determined by the time that is needed to create a high-quality image, which depends on the exposure time required for contrast, and the time required for the specimen to be (near) motionless in the view of the camera. Given the increasing demands from industry, there is a clear desired to improve the throughput of EMs.

☆ This work is supported by the Netherlands Organization for Scientific Research (NWO-TTW) under grant number 12697 "Control based on Data-Intensive Sensing," and by the Innovational Research Incentives Scheme under the VICI grant "Wireless control systems: A new frontier in automation" (No. 11382) awarded by NWO-TTW.

* Corresponding author.
E-mail address: eelcovanhorssen+tue@gmail.com (E.P. van Horssen).

https://doi.org/10.1016/j.ifacsc.2020.100074
2468-6018/

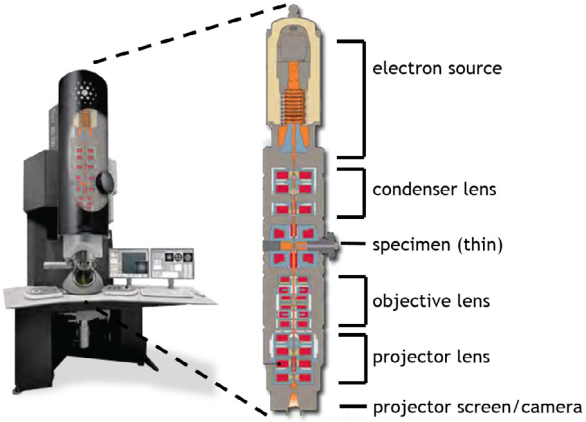

Fig. 1. Main components of a transmission electron microscope (TEM) system (adapted from FEI, 2010). A beam of electrons emitted from a source is guided by lens systems through a specimen that is imaged on a projector screen or camera.

One of the bottlenecks in improving throughput is *drift*, a phenomenon inherent to the current EM systems, which is a collective term for several disturbance processes. Drift induces a (very) slowly fading motion of the specimen, which causes blurring of the image, because it corrupts the electron detection process and therefore the image-acquisition process itself. Reducing the exposure time limits the drift effect but also the image contrast, and thus also makes high-quality imaging infeasible. Waiting for the drift to fade significantly limits the throughput of images, but is current state-of-the-art in EM practice. Hence, counteracting drift could be one of the enablers to increase throughput, while preserving high-quality imaging.

In order to provide even better products for their customers, Thermo Fisher Scientific envisions feedback control to correct for drift as a means to improve imaging quality and throughput beyond current limits imposed by drift in their systems. The introduction of a controlled actuation system, called 'stage', to move the specimen holder during the imaging process provides a promising alternative to the conventional "waiting" before the specimen comes to standstill by itself. To support this vision, this paper present a modeling and control methodology that allows to move the stage to correct for drift and make the specimen (nearly) motionless in the view of the camera.

The focus in this paper will be on the imaging effects in TEM systems, which takes full-resolution images, although the authors believe that the results in the paper, can also benefit scanning-type EMs on an image-to-image timescale. If pixel-to-pixel tracking algorithms can provide fast enough drift estimates, and provided that the control system is fast enough, the methodologies in this paper could be applied to correct for drift during the scanning process. Here, we consider image-to-image tracking algorithms with a well-defined finite completion time for given imaging settings.

Throughout this paper, as a representative industrial example and case study, an electron microscope image of gold (courtesy of Thermo Fisher Scientific) will illustrate the problems in imaging with disturbances. Fig. 2 depicts how image quality changes when Poisson noise affects the electron detection process, and how drift creates a blurring effect. A field-of-view (FOV) around a point-of-interest (POI) of the object is shown. The first picture (a) can only be obtained after a long exposure time without drift, the other pictures (b) and (c) can be observed after a shorter exposure time without and with drift, respectively. Clearly, much contrast is lost due to drift. Since the images themselves are corrupted by drift,

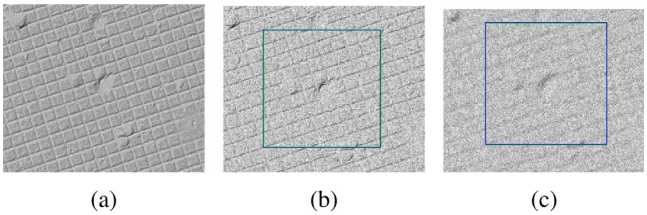

Fig. 2. Object (gold) in high contrast (a), in low contrast image affected by Poisson noise without blur (b), and with blur (c). (For interpretation of the references to color in this figure legend, the reader is referred to the web version of this article.)

post-processing cannot be used to adequately correct for it. From observations at Thermo Fisher Scientific and their customers, this drift is quite unpredictable and it is aggressive at first, but becomes less aggressive as time progresses. Therefore, the quality of the images improves over time if the system is not otherwise disturbed. Typically, after a specimen has been placed in the EM at least several minutes of waiting time are required before any (low quality) image information can be obtained. This waiting time varies from minutes to more than a day, depending on the working setting. Often, it even occurs that the POI (almost) leaves the FOV. If the POI leaves the FOV, at present a highly-trained human operator may manually perform a rough correction for the drift by controlling a joystick that moves the stage. Such an operation by a human operator may, unfortunately, introduce additional drift. In fact, in many cases, the initial drift is too random and too fast for a human operator to correct for and waiting is required. In current practice, online corrections during the imaging process are not performed.

Given the above issues, our objective is to realize an automated drift compensation system based on this stage and the online analysis of images to obtain measurements of the motion of the POI, which thereby acts as an image-based soft sensor. We stress again that the image-based sensor is the only means to obtain estimates of the drift at the microscopic level, especially if sub-Ångström resolutions are desired. We follow a model-based design approach, which takes into account a model for the disturbances. In fact, some characteristics of the disturbances, which will be discussed in more detail in Section 2, are known.

1.2. Related work

Some approaches for control in (electron) microscopes related to our work have been proposed in the literature. To coordinate low-level and high-level control of actuators in a TEM system, a hierarchical MPC-based control design was proposed (Doornbos & van Loo, 2012; Tarău, Nuij, & Steinbuch, 2011) without further study of drift. Automation for remote operation was investigated in O'Keefe et al. (1996). The papers (Andersson & Abramovitch, 2007; Andersson & Park, 2005) studied smart scanning methods to decide where in the operating area to sample. In Elmokadem and Yu (2015) a drift estimation method based on Bayesian inference was proposed. Recent works (Jin & Li, 2015; Zhang, Long, Liu, Zhang, & Feng, 2016) studied compensation of thermal drift and distortions by beam-steering in scanning microscopes. Typically, post-processing methods (Gonzalez & Woods, 2006; Salmons, Katz, & Trawick, 2010; Sutton, Orteu, & Schreier, 2009) are already used in EM systems, but these are not sufficient to compensate for all aberrations caused by drift.

1.3. Contributions

In this work, we propose a vision-based feedback controller for the stage (see Fig. 3) in order to compensate online for the drift

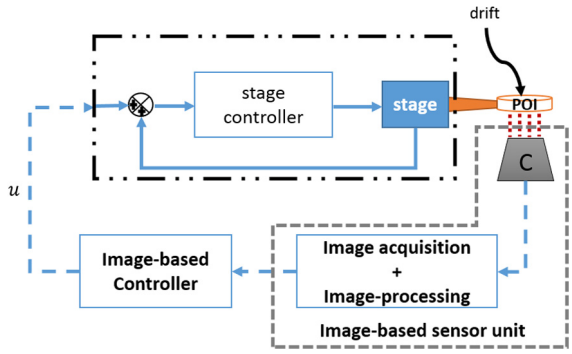

Fig. 3. Image-based feedback loop with object actuation.

disturbances, which leads to improved imaging throughput and quality. The first contribution is the mathematical formalization of the imaging improvement problem as a stochastic optimal control problem. Based on this formalized problem and modeling framework, several control design approaches could be taken. We propose a linear quadratic Gaussian(LQG)-type solution to this problem, which follows as a natural choice for the seemingly stochastic nature of the drift and the resulting stochastic optimal control problem. In particular, we will use the modeling approach proposed in van Horssen, Antunes, and Heemels (2015, 2019) for which the data-acquisition method consists of the imaging process as well as the tracking process. The application of LQG-type control design in this industrial context is the second contribution. Moreover, we show as a third contribution how the switching approach introduced in van Horssen et al. (2015, 2019) can enhance performance even further by switching online between different sets of sensing parameters, i.e., with different data-acquisition settings. Note that we do not focus on improving the image-processing methods themselves. A strong feature of the applied method is not only the fact that performance may improve, but also that the method is guaranteed not to lose performance when switching, which is not guaranteed for switching control methods in general (Geromel, Deaecto, & Daafouz, 2013). Since multirate control is an often-used approach when timing issues arise, our fourth contribution is a formalized multirate solution in the industrial context of this paper. Our fifth contribution is a simulation environment to test closed-loop control of an electron microscope with simulated industrial disturbances using an image-based measurements system with industrial tracking software by using benchmark industrial images, which we apply to a case study that is highly relevant for our industrial partner. The simulator includes image aberrations by including a Poisson process for the camera exposure process and a Gaussian blurring for motion during image acquisition. Our sixth contribution is the validation of the proposed control approaches in this industrial simulation environment.

The authors believe that this is a pioneering study of drift compensation in EMs by using optimal control tools. To aid implementation of the methods, we provide many details on the control design and propose a design flow to identify system parameters, which can be used in the simulator as well as in a real system setup. The design flow and the proposed methods are numerically illustrated in the newly developed simulation environment by a representative case study of an EM model, which is a seventh and final contribution.

1.4. Outline of the paper

The organization of the remainder of the paper is as follows. Section 2 provides an overview of the experimental system, the drift model, and the main problem formulation. Section 3 presents the formal control design problem. Control solutions for processing delay smaller and larger than one sensing interval are presented in Sections 4 and 5, respectively. Section 6 gives details on the electron microscope simulator environment and presents numerical results of a relevant industrial case study to illustrate the control designs. Concluding remarks are given in Section 7.

2. System description and problem formulation

This section provides details on the main components of the electron microscope system that were described in the introduction and presents the main problem that is addressed in this work.

2.1. System overview

Fig. 3 illustrates the setup under consideration in this paper. A point $p_{POI} \in \mathbb{R}^{n_p}$ on an object in the view of the camera is chosen as the Point-Of-Interest (POI). The object is placed on a holder, which is connected to a motion-controlled 'stage'. A low-level stage controller receives setpoints from an image-based controller and positions the stage based on position measurements from the stage and this setpoint information. Drift affects the position of the POI, which cannot be measured by the stage measurement system. To obtain drift information, an observation system in the form of an image-based sensor unit registers changes in the position of the POI. In this image-based sensor unit, camera images are acquired by dedicated hardware and processed by a visual tracking system resulting in a position measurement of the POI. Based on this POI position information, the image-based controller in Fig. 3, detailed in the sequel, decides on motion setpoints, which are fed to the stage to counteract the drift motion of the object with respect to the camera.

Deviations from the initial position of p_{POI} in the field of view of the camera are described by the position error

$$e(t) := p_{POI}(t) - p_{POI}(0), \qquad t \in \mathbb{R}_{\geq 0}, \tag{1}$$

where $e(t) \in \mathbb{R}^{n_p}$. Recall that we select $p_{POI}(0)$, and as such it is exactly known.

In this work, we address multiple-input multiple-output (MIMO) systems for reasons of generality, since such systems are typically of interest in vision-based control. For ease of exposition, we illustrate the ideas and results for a single-input single-output (SISO) system with $n_p = 1$.

2.2. Observation system and error model

The observation system in the form of an image-based sensor unit can be divided into a camera, an image-acquisition system and image-processing.

2.2.1. Camera and image acquisition

The camera captures grayscale images of $\mathbf{w} \times \mathbf{h}$ pixels, $\mathbf{w}, \mathbf{h} \in \mathbb{N}$. The imaging accuracy of the system is expressed as the resolution $r \in \mathbb{R}$, which determines how much of the object is displayed by one pixel, e.g., a resolution of 0.1 nm/pixel means that an area on the specimen of 0.1 by 0.1 nanometer is imaged in one pixel. Camera images are obtained at a frequency of $f^c \in \mathbb{R}_{>0}$ Hz. The time between camera images is given by $\tau^c := \frac{1}{f^c}$, which is the minimal exposure time of the camera. The imaging process can be considered as an electron counting process that works at low exposure levels with an average doserate of $DR \in \mathbb{R}_{>0}$ electrons per pixel per second, which depends on the electron beam strength and the type of specimen. The intensity of a pixel in an image is given by the actual number of electrons that are

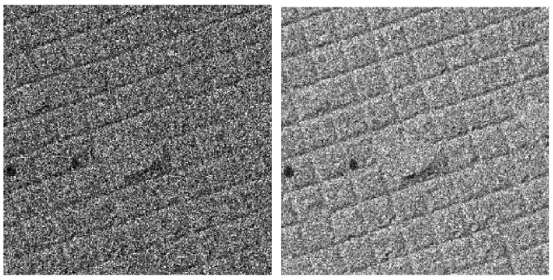

Fig. 4. Templates with low contrast (left, low N^e, fewer intensity levels) and high contrast (right, high N^e, more intensity levels).

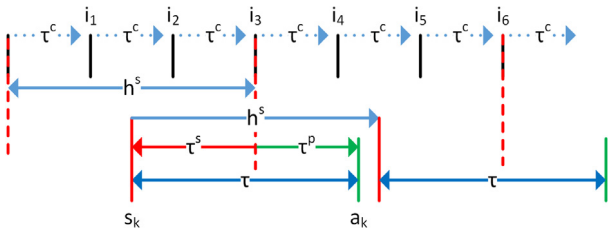

Fig. 5. Sensing timing for three exposure intervals combined ($N^i = 3$): imaging instants i_n, $n = 1, \ldots, 6$, sensing moment s_k, actuation moment a_k.

counted. During an exposure of τ^c seconds, the average number of electrons detected per pixel in the camera is given by $N^e_{min} := \tau^c \times DR$. The actual pixel intensity depends on the specimen and the electron arrival process. The number of arriving electrons per pixel can be modeled as a Poisson process. Hence, we say that the pixel intensity is corrupted by Poisson noise.

The output of the image-acquisition system is called a *frame*, i.e., an image of a desired level of quality that is obtained with a desired exposure time. Here, we discuss the imaging process itself and, for now, neglect the blurring effect of drift, which is discussed in more detail in Sections 2.4 and 2.5. The quality of the frame can be assessed by its contrast. The contrast increases with the average number of electrons that are counted. Hence, in order to improve quality, we can count over longer exposure times, which are restricted to durations that are multiples of τ^c. This increases image quality (and therefore the expected position measurement accuracy) but comes at the cost of a larger delay before information becomes available. In practice, the frame generation for multiple intervals τ^c is realized by either combining multiple images taken at rate τ^c (i.e., summing the pixel values) or by increasing the exposure time in the electron counting process, leading to similar resulting frames. In this work, we consider the first case in which multiple images are combined. For $N^i \in \mathbb{N}$ imaging intervals combined, the average number of electrons counted per pixel is $N^e := N^i \times N^e_{min}$ and the total frame acquisition time is $h^s := N^i \times \tau^c$ seconds. The blurring effect of drift reduces the image contrast. Therefore, reducing the drift effect also benefits the imaging process.

2.2.2. Image-processing

The image-processing step takes the acquired images/frames and uses a feature tracker to identify deviations in the position of a 'template' with respect to its expected position. Using a 'first' frame, the feature tracker decides (possibly with the help of an operator) what the point of interest on the specimen is, and thereby the position $p_{POI}(0)$ in the frame. The template is a section of the initial image around the POI (or around some feature near it). Such templates of 256 × 256 pixels are depicted in Fig. 4 for variations in N^e, which are sections of larger frames as depicted in Fig. 2 by the green/blue squares.

The image-processing method used in this work is a normalized cross-correlation filter with subpixel accuracy detailed in Guizar-Sicairos, Thurman, and Fienup (2008) as the single-step DFT algorithm. Input for the image-processing is the original template and a new frame. This algorithm returns the position of the template in the new frame by an optimization over a subpixel approximation (with a predefined accuracy), and it does this in all subsequent frames. In this work, we aim to present control design ideas rather than improvements in data-processing. Hence, instead of searching for the best image-processing algorithm, we assume the image-processing method to be given by the method in Guizar-Sicairos et al. (2008). In the actual system, the tracker is implemented in dedicated hardware such that the computational time can be assumed constant.

2.2.3. Sampling intervals and measurement accuracy

Using the tracker, the error e in (1) is observed/measured at discrete *sensing instants* $s_k \in \mathbb{R}_{\geq 0}$, $k \in \mathbb{N}$ leading to the *sampling intervals*

$$h^s_k := s_{k+1} - s_k \in \mathbb{R}_{>0},\ k \in \mathbb{N}. \tag{2}$$

We assume that a sensing instant corresponds to the central time in the electron counting process, leading to a sensing delay $\tau^s_k = \frac{h^s_k}{2}$ equal to the difference between the central time and the moment the last image in the series of length N^i is obtained, i.e., the moment that the new frame is available. In this work, we consider a blurring effect for the total motion during acquisition such that the central time is the most natural choice. However, our control approaches can easily be adapted to other choices of the sampling instants, such as the start or end of the acquisition time, as well. Traditionally, the system operates at a fixed rate consistent with the acquisition time, i.e., $h^s_k = h^s$ for some fixed h^s for all $k \in \mathbb{N}$. In this work, however, we will also deviate from traditional operation and switch between different sensing and actuation rates, as will be discussed in the sequel. In Fig. 5, the sensing instants are depicted for the traditional case with three exposure intervals combined ($N^i = 3$). After a new frame is acquired, the measurement of the error

$$y_k = e_k + v_k, \qquad k \in \mathbb{N}, \tag{3}$$

where e_k denotes $e(s_k)$, becomes available after a processing delay $\tau^p \in \mathbb{R}_{>0}$. Recall that the processing delay is a fixed constant, i.e, it does not depend on the sensing interval. The measurements are corrupted by measurement noise $v_k \in \mathbb{R}^{n_p}$. We assume that the Poisson noise at the pixel level results in a Gaussian deviation in the measurements. In other words, the measurement noise is assumed to be zero-mean additive Gaussian white noise (AGWN), i.e., v_k is a zero-mean Gaussian random variable with variance V_k. This assumption will be validated through the analysis of sequences of frames.

We take the *actuation update instants* $a_k \in \mathbb{R}_{\geq 0}$, $k \in \mathbb{N}$, to be equal to the moments at with measurements y_k, $k \in \mathbb{N}$, become available. The total delay between the sensing instant s_k and the corresponding actuation instant a_k is then given by

$$\tau_k = \tau^s_k + \tau^p = \frac{h^s_k}{2} + \tau^p, \qquad k \in \mathbb{N}, \tag{4}$$

corresponding to the time between the central acquisition time and the end of the processing. When the system operates at a fixed rate, this total sensing-to-actuation delay is fixed and denoted by τ, see also Fig. 5.

2.3. Actuation system

The actuation system or *stage* consists of a moving part, the specimen holder, which moves with respect to the camera, and a

mechanically fixed part that is not moving with respect to the camera, which enables relative motion of the specimen in the view of the camera. A stage controller, see Fig. 3, uses direct measurements of the stage, for example, the position $p_s(t) \in \mathbb{R}^{n_u}, t \in \mathbb{R}_{\geq 0}$, to accurately follow setpoints of up to 4th order derivatives of a reference position $p_s^{ref}(t) \in \mathbb{R}^{n_u}, t \in \mathbb{R}_{\geq 0}$. We assume that $n_u = n_p$, such that we can set one derivative of the position for each dimension of the position error (confer (1)). Later, in Section 2.6, we will detail which derivative is most suitable and use that reference setpoint as the control input for the image-based feedback loop.

We assume the stage system to be a well-tuned closed-loop system that can be assumed ideal with respect to the image-based feedback loop, i.e., a time scale separation exists between the stage control loop and the image-based control loop. Note that if this assumption is not valid, an appropriate model, for example, a more complex state–space model of the stage control loop, may be included in the modeling and design steps that are proposed next.

Assumption 1. The stage perfectly follows a given setpoint, i.e., $p_s = p_s^{ref}$.

We further assume that initially the stage is at standstill at $p_s(0) = p_s^{ref}(0)$.

Stage movements are (to be) kept relatively small such that there are no mechanical vibrations excited in the holder. Furthermore, the actuation system only allows for digital updates of the actuation setpoint at discrete-time actuation update instants $a_k \in \mathbb{R}_{\geq 0}, k \in \mathbb{N}$ and we have a standard zero-order hold approach between actuation update instants.

Note that the *actuation intervals* $h_l^a = a_{l+1} - a_l \in \mathbb{R}_{>0}, l \in \mathbb{N}$ need not be equal to the sampling intervals. At first, we will assume that there is one actuation update per sample, which takes place after the processing delay τ_k, i.e., $a_k = s_k + \tau_k$ for all $k \in \mathbb{N}$. We then have *actuation intervals* $h_k^a = a_{k+1} - a_k \in \mathbb{R}_{>0}, k \in \mathbb{N}$, and we propose control designs for the case where $h_k^a = h_k^s$ for all $k \in \mathbb{N}$. When the actuation rate is fixed, we omit the subscript k or l and denote the actuation interval by h^a. Afterwards, in Section 4.5, we also propose a multirate approach where actuation is faster than sampling, which leads to actuation intervals h_k^a shorter than the sampling intervals h_k^s.

We assume that the control computation delay is negligible compared to the acquisition and processing delay τ_k.

2.4. Drift effect and motion blur

We assume that all changes in p_{POI} in the images are either a result of movements of the stage or of the disturbances causing differences between p_s and p_{POI}. Those disturbances are jointly modeled as drift $d(t) \in \mathbb{R}^{n_p}$ in position for all $t \in \mathbb{R}_{\geq 0}$, i.e.,

$$e(t) := p_{POI}(t) - p_{POI}(0) = p_s(t) - p_s(0) + d(t). \tag{5}$$

In the next subsection, we present a dynamic model for the (drift) disturbance d.

In practice, motion of the object during image acquisition results in blurring effects in the frames. We consider the motion blur to manifest as a Gaussian filtration of the image with zero-mean and standard deviation equal to the total movement in pixels between obtained frames.

2.5. Disturbance model

As mentioned before, some characteristics of the disturbance are known. Based on insights from industrial experts, we propose an approximate model of the total movement due to drift $d(t) \in \mathbb{R}^{n_p}$ for all $t \in \mathbb{R}_{\geq 0}$. Recall that, for simplicity, we consider $n_p = 1$ in this work, although generalizations to higher dimensions are straightforward.

One of the main causes of the disturbance is internal thermal drift, which occurs in the system and in the specimen itself, at frequencies up to 1 Hz. Other external disturbances, which typically occur at higher frequencies, can often be well-addressed by other measures taken on the working site of the EM system, such as active vibration isolation. Therefore, we focus here on the internal drift type disturbance. The main component of the drift is a continuous motion in one unknown major direction in $\mathbb{R}^{n_p}$, with small variations in a short period (e.g., up to several minutes), but the movement speed is exponentially decaying over longer periods ($>$ 1000 min). For control purposes, we can consider the behavior over a shorter period. Hence, we can assume that the major drift component is a constant speed in one major direction and that this main drift is randomly perturbed, which can be on any time scale. We assume, based on insights from industrial experts, that an accurate drift model for $n_p = 1$ is given by the following second order stochastic differential equation, which can capture many variations of drift:

$$\ddot{d}(t) = \underbrace{0}_{\text{constant speed}} + \underbrace{B_{w^d} \frac{dw^d}{dt}}_{\text{small perturbations}}, \tag{6}$$

where w^d is a one-dimensional Wiener process with incremental covariance (Åström, 1970) and the gain B_{w^d} of the random Wiener process models the variations in the speed. The differential equation (6) can be expressed in state–space form as

$$\begin{bmatrix} \dot{d} \\ \ddot{d} \end{bmatrix} = \begin{bmatrix} 0 & 1 \\ 0 & 0 \end{bmatrix} \begin{bmatrix} d \\ \dot{d} \end{bmatrix} + \begin{bmatrix} 0 \\ B_{w^d} \end{bmatrix} \frac{dw^d}{dt}, \tag{7}$$

The initial condition

$$\begin{bmatrix} d(0) \\ \dot{d}(0) \end{bmatrix} = \begin{bmatrix} 0 \\ d_0^v \end{bmatrix} \tag{8}$$

models the almost constant initial drift velocity by $d_0^v \in \mathbb{R}$, which is unknown.

In this work, for ease of exposition, we assume the drift to have an effect only in one direction ($n_p = 1$). Using the insights in this paper, the methods proposed in this work can readily be extended to compensate for multi-directional drift as well.

2.6. Acceleration control

Since we can control the stage position reference up to 4th order, we have direct control over either $\dot{p}_s^{ref}(t)$, $\ddot{p}_s^{ref}(t)$, $\dddot{p}_s^{ref}(t)$, or $\ddddot{p}_s^{ref}(t)$, and thus by Assumption 1 over $\dot{p}_s(t)$ or higher order derivatives, respectively. From (5) and (6), we can see that velocity of the stage can directly compensate for the main constant drift speed if it is known. However, the drift speed is corrupted due to the small time-varying perturbations in (6) and therefore only approximately known from the measurements. Hence, to achieve compensation for the velocity and the small perturbations in (6), we select to control the acceleration of the stage $\ddot{p}_s^{ref}(t)$, i.e., $u(t) = \ddot{p}_s^{ref}(t), t \in \mathbb{R}$.

2.7. System performance

A measure for the performance is the average deviation of the POI from its initial position, which is given by the error e. This measure reflects the amount of displacement during imaging and, hence, the image quality. To prevent large control actions (which could induce additional drift), we also penalize the control input, which is a function u of the reference of the stage position,

i.e., (derivatives of) p_s^{ref}. The control performance over some time interval $[0, T]$ is measured by

$$J_T := \frac{1}{T}\int_0^T \mathbb{E}[e(t)^\intercal Q_e e(t) + u(t)^\intercal R_u u(t)]dt \tag{9}$$

with $Q_e \in \mathbb{S}_+^{n_p}$, $R_u \in \mathbb{S}_+^{n_u}$, where $\mathbb{S}_+^n$ denotes symmetric positive definite matrices of dimension $n \times n$ and $\mathbb{E}[\cdot]$ denotes expectation. For the one-dimensional system considered in this work, we select $Q_e = 1$ and tuning involves only the parameter $R_u \in \mathbb{R}_{>0}$.

In this work, we consider a stabilization problem of the error over periods of time much larger than the sensing intervals. Therefore, T in (9) can be assumed infinite and we will consider infinite horizon control designs based on performance measure $J := \lim_{T\to\infty} J_T$.

Control designs for infinite T typically perform well even in finite horizon problems. Nevertheless, finite horizon counterparts for the design may be directly deduced from the equations in this work and the derivations in van Horssen et al. (2019). Note that switching conditions that are explicitly derived for the finite horizon case will be more involved in terms of computations (see also van Horssen et al., 2019). Using a meaningful final cost is important in the finite horizon case.

2.8. Problem formulation and approach

Formally, the main goal considered in this work is the reduction of performance measure (9) for $T \to \infty$ in comparison to the uncontrolled case, meaning that the POI is stabilized close to its initial position (which can be selected arbitrarily) by a model-based design of an image-based feedback controller (as in Fig. 3).

The approach we take to solve the problem will address the following challenges:

(1) Establish an appropriate model of the open-loop system.
(2) Model-based design of image-based feedback controllers.
(3) Validation of the control design.

In this paper, we tackle these challenges in the order in which they are presented. The first challenge is already partly addressed in the first part of the paper. Firstly, we established (3) as the measurement model. Second, we proposed a model for the error (5) and a model (6) for the drift disturbance. Next, we illustrate how we can establish an open-loop model and how we can use that model in control design. In particular, by using the framework presented in van Horssen et al. (2015, 2019), we design controllers that take into account the drift, the measurement inaccuracies, and the delay. Note that most works in the vision-based control literature do not explicitly address the delay caused by processing (Corke, 2011; Se, Lowe, & Little, 2005), whereas van Horssen et al. (2015, 2019) aimed to exploit knowledge about the delay instead and study the relation with accuracy of the processed measurement, which was studied by Krautgartner and Vincze (1998) and Sharkey and Murray (1996) in a different context as well. Lastly, we present an industry-based simulator to test open-loop and closed-loop behavior of an electron microscope system with image-based feedback to illustrate and validate our designs.

3. Formalizing the control design problem

Using the models proposed in the previous section, we can design controllers for the system with measurement delay. To formalize the control design problem, we give a state–space representation of the open-loop system and a discretization.

3.1. Open-loop state–space system model

The ideal dynamics of the error system are given by

$$\dot{e} = \dot{p}_{POI} = \dot{p}_s + \dot{d} = \dot{p}_s^{ref} + \dot{d}, \tag{10}$$

which follows from (1) and (5). For generality, we can include an additional Wiener process w^e for any additional unmodeled perturbations on the position of the POI. The open-loop system, taking into account (7), can then be represented in state space as

$$\begin{bmatrix} \dot{e} \\ \ddot{d} \\ \ddot{p}_s^{ref} \end{bmatrix} = \begin{bmatrix} 0 & 1 & 1 \\ 0 & 0 & 0 \\ 0 & 0 & 0 \end{bmatrix} \begin{bmatrix} e \\ \dot{d} \\ \dot{p}_s^{ref} \end{bmatrix} + \begin{bmatrix} 0 \\ 0 \\ 1 \end{bmatrix} u + \begin{bmatrix} B_{w^e} & 0 \\ 0 & B_{w^d} \end{bmatrix} \begin{bmatrix} \frac{dw^e}{dt} \\ \frac{dw^d}{dt} \end{bmatrix},$$

which can be rewritten as

$$\underbrace{\begin{bmatrix} \dot{e} \\ \ddot{d} + \ddot{p}_s^{ref} \end{bmatrix}}_{\dot{x}} = \underbrace{\begin{bmatrix} 0 & 1 \\ 0 & 0 \end{bmatrix}}_{A_c} \underbrace{\begin{bmatrix} e \\ \dot{d} + \dot{p}_s^{ref} \end{bmatrix}}_{x} + \underbrace{\begin{bmatrix} 0 \\ 1 \end{bmatrix}}_{B_c} u + \underbrace{\begin{bmatrix} B_{w^e} & 0 \\ 0 & B_{w^d} \end{bmatrix}}_{B_w} \underbrace{\begin{bmatrix} \frac{dw^e}{dt} \\ \frac{dw^d}{dt} \end{bmatrix}}_{\frac{dw}{dt}}, \tag{11}$$

where the system can be written with state $x := [\ e\ ,\ \dot{d} + \dot{p}_s^{ref}\ ]^\intercal$, and thus more compactly, as

$$\dot{x} = A_c x + B_c u + B_w \frac{dw}{dt}, \tag{12}$$

where w is an n_w-dimensional Wiener process and (A_c, B_c) is controllable.

The measurements are given by

$$y_k = Cx(s_k) + v_k, \tag{13}$$

where $C = [1\ 0]$ and v_k is a zero-mean Gaussian random variable with variance V_k. The variance V_k represents the accuracy of the measurements, which depends on the data acquisition settings, as explained in Section 2.

The performance (9) can be expressed as a standard linear quadratic Gaussian (LQG)-type average cost function (Åström, 1970)

$$J_T = \frac{1}{T}\int_0^T \mathbb{E}[g_c(x(t), u(t))]dt, \tag{14}$$

where $g_c(x, u) := x^\intercal Q_c x + u^\intercal R_c u$ with positive definite matrix $R_c \succ 0$, and positive semi-definite matrix $Q_c \succeq 0$. In particular, we have

$$Q_c = \begin{bmatrix} Q_e & 0 \\ 0 & 0 \end{bmatrix}, \qquad R_c = R_u, \tag{15}$$

with $(A_c, Q_c^{1/2})$ observable.

3.2. Discretization

We assume $s_0 = 0$ and the first actuation update is thus delayed by a_0. A standard zero-order hold sampled-data (Åström & Wittenmark, 2013) approach is taken between actuation update instants, i.e.,

$$u(t) = u_k, \qquad \text{for all } t \in [a_k, a_{k+1}), \tag{16}$$

where $u_k := u(a_k)$ and $u(t) = u_{-1} := 0$ for all $t \in [0, a_0)$.

Let $x_k := x(a_k)$ denote the state at the actuation update instants for all $k \in \mathbb{N}$. By discretization of the system (12) at times a_k, $k \in \mathbb{N}$, we obtain

$$x_{k+1} = A(h_k^a)x_k + B(h_k^a)u_k + w_k, \tag{17}$$

where $A(h) := e^{A_c h}$ and $B(h) := \int_0^h e^{A_c s} B_c ds$. The Wiener process can be represented in discrete time by a sequence of Gaussian

zero-mean independent random vectors $w_k \in \mathbb{R}^{n_w}$, $k \in \mathbb{N}$, with covariance $\mathbb{E}[w_k(w_k)^\intercal] = W(h_k^a)$, where $W(h) := \int_0^h e^{A_c s} B_w B_w^\intercal e^{A_c^\intercal s} ds$.

The average cost (14), for $T = a_0 + \sum_{k=0}^{N-1} h_k^a$, $N \in \mathbb{N}_{>0}$, can be written as

$$J_T = \frac{1}{a_0 + \sum_{k=0}^{N-1} h_k^a} \mathbb{E}\left[g(x(0), u(0), a_0) + \sum_{k=0}^{N-1} g(x_k, u_k, h_k^a) \right], \quad (18)$$

where $g(x, u, h) := x^\intercal Q(h) x + 2x^\intercal S(h) u + u^\intercal R(h) u + \alpha(h)$, with

$$\begin{bmatrix} Q(h) & S(h) \\ S(h)^\intercal & R(h) \end{bmatrix} := \int_0^h e^{\begin{bmatrix} A_c & B_c \\ 0 & 0 \end{bmatrix}^\intercal s} \begin{bmatrix} Q_c & 0 \\ 0 & R_c \end{bmatrix} e^{\begin{bmatrix} A_c & B_c \\ 0 & 0 \end{bmatrix} s} ds,$$

and, for $tr(\cdot)$ denoting the trace of a matrix,

$$\alpha(h) := tr(Q_c \int_0^h \int_0^t e^{A_c s} B_w B_w^\intercal e^{A_c^\intercal s} ds dt),$$

which is the cost associated with the continuous-time behavior of the Wiener process between update instants.

Note that, for the system with one-dimensional drift, the matrices of the discrete-time dynamics with time interval h can analytically be computed to be equal to

$$A(h) = \begin{bmatrix} 1 & h \\ 0 & 1 \end{bmatrix}, B(h) = \begin{bmatrix} \frac{h^2}{2} \\ h \end{bmatrix},$$

$$W(h) = \begin{bmatrix} B_{w^e}^2 h + \frac{B_{w^d}^2 h^3}{3} & \frac{B_{w^d}^2 h^2}{2} \\ \frac{B_{w^d}^2 h^2}{2} & B_{w^d}^2 h \end{bmatrix},$$

$$\alpha(h) = \frac{1}{12} Q_e \left(6 B_{w^e}^2 h^2 + B_{w^d}^2 h^4 \right).$$

3.3. Control problem

We formulate here the control problem for $h_k^s = h_k^a$ for all $k \in \mathbb{N}$, which can be generalized to the multirate case in a straightforward manner. The information set available to the controller at time a_k, $k \in \mathbb{N}$, is given by

$$\mathrm{I}_k = \{y_k\} \bigcup \{u_{k-1}, h_{k-1}^a, \mathrm{I}_{k-1}\} \text{ with } \mathrm{I}_0 = \{y_0, u_{-1}, a_0, s_0\}.$$

The control problem is the design of the inputs u_k and the selection of the data-acquisition intervals h_k^s / h_k^a such that (18) is minimized. Observe that (17) is an LTI discrete-time system if $h_k^a = h^a$ is fixed for all $k \in \mathbb{N}$, which results in an LQG-type design problem. Recall that we assume T to be very large, and we aim to minimize $J := \lim_{T \to \infty} J_T$. It follows from dynamic programming (see, e.g., Bertsekas, 2005), that the optimal control input u_k minimizes $\mathbb{E}\left[g(x_k, u_k, h^a) + V(x_{k+1}) \mid \mathrm{I}_k \right]$, where $V(x) = x^\intercal P x$ for some $P \succeq 0$. Recall that we have sensing-to-actuation delay and partial measurements. From, e.g., Åström (1970) it is known that the separation principle holds if $h_k^a = h_k^s$ for all $k \in \mathbb{N}$. Thus, when $h_k^a = h_k^s = h^s = h^a$ is fixed for all $k \in \mathbb{N}$, we can design an optimal controller in the form of a state feedback regulator and a state estimator that can be computed separately by solving algebraic Riccati equations, as detailed in the next sections.

Optimization of both the inputs u_k and h_k^s for an infinite (or large) number of sampling instants results in a combinatorial problem for which no tractable and optimal solutions are known to exist. Hence, we propose a suboptimal switched control design based on van Horssen et al. (2019), which is guaranteed to perform at least as good as the best non-switched design and can provide improvements nonetheless. Furthermore, we first consider the case where $\tau < h^s$ in Section 4. Later, in Section 5, we discuss the case $\tau > h^s$.

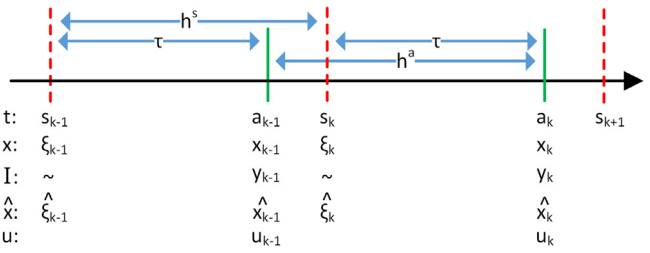

Fig. 6. Timings for control under small delay.

4. Control design for $\tau < h^s$

We first present the optimal control design for a non-switching strategy, based on the assumption that $h_k^a = h_k^s = h^s = h^a$ is fixed for all $k \in \mathbb{N}$. From a performance analysis of this control design, we can determine the optimal choice $h_\star \in \mathbb{R}_{>0}$ of a fixed sampling interval, i.e., we can determine the optimal value of the exposure time of the system for the case that $h_k^a = h_k^s = h_\star$ for all $k \in \mathbb{N}$. Subsequently, we present switching conditions to select online at time a_k the next interval $h_k^s = h_k^a$ and the corresponding measurement accuracy V_k in order to improve performance. Finally, we present a multirate design for faster actuation, i.e., $h^s > h^a$. We assume here that the processing delay is less than the sampling interval, as depicted in Fig. 6.

4.1. Optimal regulator

Here, we assume that we have an estimate $\hat{x}_k := \mathbb{E}[x_k \mid \mathrm{I}_k]$ of the full state available at a_k. If the estimator is optimal, then the optimal regulator is given, for all $k \in \mathbb{N}$, by

$$u_k = -K \hat{x}_k. \quad (19)$$

The control gain K is obtained by solving, for positive definite P, the Riccati equation

$$P = A(h^a)^\intercal P A(h^a) + Q(h^a) - K^\intercal G K$$
$$K = G^{-1}(B(h^a)^\intercal P A(h^a) + S(h^a)^\intercal)$$
$$G = B(h^a)^\intercal P B(h^a) + R(h^a).$$

4.2. Optimal estimator

The estimate $\hat{x}_k = \mathbb{E}[x(a_k) \mid \mathrm{I}_k]$ can be obtained by an estimator–predictor design. Note that u_{k-1} is known after a_{k-1}. We first recall that y_k is a measurement of the error delayed by τ w.r.t. a_k. The estimate at actuation time can be expressed as a function of the state estimate at sampling time as

$$\begin{aligned} \hat{x}_k &= \mathbb{E}[x(a_k) \mid \mathrm{I}_k] \\ &= \mathbb{E}[A(\tau) x(s_k) + B(\tau) u_{k-1} + w(s_k, \tau) \mid \mathrm{I}_k] \\ &= A(\tau) \mathbb{E}[x(s_k) \mid \mathrm{I}_k] + B(\tau) u_{k-1} \\ &= A(\tau) \xi_k + B(\tau) u_{k-1}, \end{aligned} \quad (20)$$

where $\xi_k := \mathbb{E}[x(s_k) \mid \mathrm{I}_k]$ is the estimate of the state at the sampling instant after y_k has arrived at the controller and where $w(s_k, \tau)$ is a zero-mean Gaussian disturbance with covariance $W(\tau)$. This is a pure prediction step.

The variance of the estimate is given by

$$\begin{aligned} \Theta_k^a &:= \mathbb{E}[(x(a_k) - \hat{x}_k)(x(a_k) - \hat{x}_k)^\intercal \mid \mathrm{I}_k] \\ &= \mathbb{E}[A(\tau)(x(s_k) - \xi_k)(x(s_k) - \xi_k)^\intercal A(\tau)^\intercal \\ &\quad + w(s_k, \tau) w(s_k, \tau)^\intercal + \mathit{crossterms} \mid \mathrm{I}_k] \\ &= A(\tau) \mathbb{E}[(x(s_k) - \xi_k)(x(s_k) - \xi_k)^\intercal \mid \mathrm{I}_k] A(\tau)^\intercal + W(\tau) \end{aligned}$$

$$= A(\tau)\Theta_k^s A(\tau)^\intercal + W(\tau), \tag{21}$$

where $\Theta_k^s := \mathbb{E}[(x(s_k) - \xi_k)(x(s_k) - \xi_k)^\intercal \mid \mathrm{I}_k]$ and the crossterms with $w(s_k, \tau)$ vanish when taking the expectation.

Since the delay is less than the actuation interval, the state estimate ξ_k is a current state estimator. However, I_k is not available at s_k. Hence, we require a predicted estimate of $x(s_k)$ after a_{k-1}, which we define as

$$\begin{aligned}\hat{\xi}_k &:= \mathbb{E}[\xi_k \mid \mathrm{I}_{k-1}] = \mathbb{E}[\mathbb{E}[x(s_k) \mid \mathrm{I}_k] \mid \mathrm{I}_{k-1}] = \mathbb{E}[x(s_k) \mid \mathrm{I}_{k-1}] \\ &= \mathbb{E}[A(h^s - \tau)x(a_{k-1}) \\ &\quad + B(h^s - \tau)u_{k-1} + w(a_k, h^s - \tau) \mid \mathrm{I}_{k-1}] \\ &= A(h^s - \tau)\hat{x}_{k-1} + B(h^s - \tau)u_{k-1}. \end{aligned} \tag{22}$$

The covariance of the predicted estimate is given by

$$\begin{aligned}\hat{\Theta}_k^s &:= \mathbb{E}[(x(s_k) - \hat{\xi}_k)(x(s_k) - \hat{\xi}_k)^\intercal \mid \mathrm{I}_{k-1}] \\ &= \mathbb{E}[A(h^s - \tau)(x(a_{k-1}) - \hat{x}_{k-1}) \\ &\quad \times (x(a_{k-1}) - \hat{x}_{k-1})^\intercal A(h^s - \tau)^\intercal \\ &\quad + w(a_k, h^s - \tau)w(a_k, h^s - \tau)^\intercal + \mathit{crossterms} \mid \mathrm{I}_{k-1}] \\ &= A(h^s - \tau)\Theta_{k-1}^a A(h^s - \tau)^\intercal + W(h^s - \tau). \end{aligned} \tag{23}$$

After the new measurement arrives, we can use an optimal observer to update the state estimate

$$\xi_k := \mathbb{E}[x(s_k) \mid \mathrm{I}_k] = \hat{\xi}_k + L_k(y_k - C\hat{\xi}_k), \tag{24}$$

where the optimal gain is given by $L_k = \hat{\Theta}_k^s C^\intercal (C\hat{\Theta}_k^s C^\intercal + V_k)^{-1}$ (see, e.g., Åström, 1970), i.e., the Kalman gain. Note that $C\hat{\xi}_k = \mathbb{E}[e_k \mid \mathrm{I}_{k-1}]$. The variance is given by

$$\begin{aligned}\Theta_k^s &:= \mathbb{E}[(x(s_k) - \xi_k)(x(s_k) - \xi_k)^\intercal \mid \mathrm{I}_k] \\ &= \mathbb{E}[(x(s_k) - \hat{\xi}_k - L_k(y_k - C\hat{\xi}_k))(\star)^\intercal \mid \mathrm{I}_k] \\ &= \mathbb{E}[(x(s_k) - \hat{\xi}_k - L_kC(x(s_k) - \hat{\xi}_k) - L_k v_k)(\star)^\intercal \mid \mathrm{I}_k] \\ &= (I - L_kC)\mathbb{E}[(x(s_k) - \hat{\xi}_k)(x(s_k) - \hat{\xi}_k)^\intercal \mid \mathrm{I}_k] \\ &\quad \times (I - L_kC)^\intercal + L_kV_kL_k^\intercal \\ &= (I - L_kC)\hat{\Theta}_k^s(I - L_kC)^\intercal + L_kV_kL_k^\intercal. \end{aligned} \tag{25}$$

Combining the above equations, we obtain the relation

$$\begin{aligned}\Theta_k^a &= A(\tau)\big[(I - L_kC)\big[A(h^s - \tau)\Theta_{k-1}^a A(h^s - \tau)^\intercal \\ &\quad + W(h^s - \tau)\big](I - L_kC)^\intercal + L_kV_kL_k^\intercal\big]A(\tau)^\intercal + W(\tau) \\ &= A(\tau)(I - L_kC)A(h^s - \tau)\Theta_{k-1}^a \\ &\quad \times A(h^s - \tau)^\intercal(I - L_kC)^\intercal A(\tau)^\intercal \\ &\quad + A(\tau)(I - L_kC)W(h^s - \tau)(I - L_kC)^\intercal A(\tau)^\intercal + W(\tau) \\ &\quad + A(\tau)L_kV_kL_k^\intercal A(\tau)^\intercal, \end{aligned} \tag{26}$$

for changes in the covariance between actuation instants. The expression (26) is similar to Joseph form (Bar-Shalom & Li, 2001) of the covariance update equation. If L_k is the optimal time-varying Kalman filter, then (25) and (26) may be simplified. If L_k is not the optimal gain, then we can use the Joseph form (26) to compute the variance update. Note that when $h_k^a = h_k^s = h^s = h^a$ is fixed for all $k \in \mathbb{N}$, (26) converges to a stationary solution with $\Theta_k^a = \Theta_{k-1}^a$.

Remark 1. If $h^s = h^a = \tau$, i.e., if the delay is exactly equal to one sampling interval, then standard equations (see, e.g., Åström, 1970) are recovered.

4.3. Performance

The optimal LQG-type control design minimizes (18) for $N \to \infty$ and the minimal value is then given by

$$J^{LQG} := \frac{1}{h^a}c^a, \;\; c^a := tr(W(h^a)P + \Theta^a K^\intercal G K) + \alpha(h^a), \tag{27}$$

where Θ^a is the converged stationary solution to (26). The contributions from the interval a_0 are reduced to zero in the infinite horizon.

The standard observability and controllability conditions are satisfied. Therefore, stabilizing solutions exist under the additional condition that the sampling is non-pathological (Chen & Francis, 1995).

4.4. Switched controller

Suppose that we are allowed to choose the number N^i online in the sense that we can decide the number of images to combine, and therefore the length of the sensing interval, for the next frame. Recall that there is a trade-off in the sense that a longer sensing interval typically results in a smaller covariance of the measurement noise if the specimen is not moving during image acquisition, i.e., due to higher contrast in the image. We design a switching law based on the switching conditions for multiple data-acquisitions methods presented in van Horssen et al. (2019), which are based on the rollout method (Bertsekas, 2005). Let there be up to $M \in \mathbb{N}_{>1}$ possible selections of the sensing interval h_k at each actuation instant. We can compute for each $m \in \{1, 2, \ldots, M\} := \mathcal{M}$ the optimal non-switching controller and a corresponding fixed observer gain $\bar{L}_m = \hat{\bar{\Theta}}^s C^\intercal (C\hat{\bar{\Theta}}^s C^\intercal + V_m)^{-1}$ where $\hat{\bar{\Theta}}^s$ follows from the stationary solution Θ^a and one step in (23).

Suppose that $b^\star \in \mathcal{M}$ minimizes (27) amongst the methods with fixed intervals. Let the corresponding actuation variables be denoted $\bar{P}, \bar{G}, \bar{K}$. Furthermore, define for all $m \in \mathcal{M}$ P_m, G_m, K_m as the one-step finite horizon solution to the standard control Riccati equation with initial condition $\bar{P}$ for a sensing/actuation interval of length $\bar{h}_m$. The corresponding delay is given by $\bar{\tau}_m$.

Then, at actuation time (when the latest measurement has arrived), we can make a decision about the next sensing moment and the next actuation time, i.e, about the next moment at which information will become available and the accuracy of that information. In van Horssen et al. (2019), a method to derive switching conditions that guarantee performance whilst achieving performance improvement is presented, specifically, the switched controller is formally guaranteed to achieve a cost J that is equal or less than the cost J^{LQG} without switching. It selects the method that is expected to yield the minimal future cost, in the sense of $\lim_{T\to\infty} J_T$, for an infinite horizon cost prediction (see van Horssen et al., 2019 for details). Based on the result in van Horssen et al. (2019), we can derive the following switching condition to determine the next sensing interval for the case in this paper. The method $\sigma_k \in \mathcal{M}$ that is expected to yield the least future cost is given by

$$\sigma_k := \arg\min_{m\in\mathcal{M}} \hat{x}_k^\intercal P_m \hat{x}_k + \eta_m(\Theta_k^a) - \frac{\bar{h}_m}{\bar{h}_{b^\star}}c_{b^\star}^a + \alpha(\bar{h}_m), \tag{28}$$

where

$$\begin{aligned}\eta_m(\Theta_k) &:= tr(\Theta_k^a P_m + \Theta_k^a K_m^\intercal G_m K_m) \\ &\quad + tr(W(\bar{h}_m)\bar{P}) + tr(Z_{b^\star}(\Theta_{k+1}^a)\bar{K}^\intercal \bar{G}\bar{K}) \end{aligned} \tag{29}$$

and[1] $Z_{b^\star}(\Theta) = vec^{-1}\left((I - \mathcal{T}_{b^\star})^{-1} vec\,(\Theta)\right)$ with

$$\mathcal{T}_m := \tilde{A}_m \otimes \tilde{A}_m, \tag{30}$$

where $\otimes$ denotes the Kronecker product and $\tilde{A}_m := A(\bar{\tau}_m)(I - \bar{L}_m C)A(\bar{h}_m - \bar{\tau}_m)$ with $\bar{L}_m$ the stationary observer gain for interval

[1] The operator $vec\,(\cdot)$ denotes the operation that stacks the columns of a matrix and vec^{-1} denotes the inverse operation.

$\bar{h}_m$. We require the computation of the one-step prediction of the variance

$$\Theta^a_{k+1} := vec^{-1}\left(\mathcal{T}_m vec\left(\Theta^a_{k+1}\right)\right) + \Psi_m, \tag{31}$$

where

$$\Psi_m := A(\tau_m)(I - \bar{L}_m C)W(h^s_m - \tau_m)(I - \bar{L}_m C)^\intercal A(\tau_m)^\intercal + W(\tau_m) + A(\tau_m)\bar{L}_m V_m(\bar{L}_m)^\intercal A(\tau_m)^\intercal.$$

The next actuation and switching instant is then given by $a_{k+1} = \bar{h}_{\sigma_k} + a_k$. The control input is given by u_k in (19) with gain K_{σ_k} and the observer gain L_k in (24) is given by $\bar{L}_{\sigma_k}$.

Remark 2. In this work, for simplicity, we use only the stationary filter gains $\bar{L}_m$ for estimation and prediction. We could also use the time-varying Kalman filter for estimation and for the first prediction step as proposed in van Horssen et al. (2019). In the setup in this work, predicting more steps with the Kalman filter could provide additional expected gain but is computationally unattractive.

Remark 3. For simplicity, we consider in this work only a one-step decision horizon for the switching. Based on van Horssen et al. (2019), this can easily be extended.

4.5. Multirate controller: faster actuation

If flexibility in the actuator allows a faster actuation update rate, a multirate controller (see, e.g., Colaneri & de Nicolao, 1995; Colaneri, Scattolini, & Schiavoni, 1990) can be designed in which h^a is smaller than h^s. Note that we consider here the non-switching multirate approach. In a general multirate approach, actuation and sampling need not be aligned or have a fractional relation between the intervals. We aim to illustrate how a multirate approach can be considered in our control design, rather than to present new mathematical theory. Therefore, for ease of exposition, we consider only actuation rates that are fixed fractions of h^s.

Let $a_{k,h} = a_k + h \times h^a$, $h \in \mathbb{N}_{(0,H-1)}$, where $H := \frac{h^s}{h^a} \in \mathbb{N}$. Then, the multirate actuation solution is to use in each corresponding interval of length h^a after $a_{k,h}$ the control input

$$u_{k,h} = -K\hat{x}_{k,h}, \tag{32}$$

where, for $h \in \mathbb{N}_{(0,H-1)}$,

$$\hat{x}_{k,h+1} := \mathbb{E}[x(a_{k,h+1}) \mid \mathrm{I}_k] = A(h^a)x(a_{k,h}) + B(h^a)u_{k,h}, \tag{33}$$

with initial value $\hat{x}_{k,0} := \hat{x}_k$. For all $k \in \mathbb{N}$, for $h \in \mathbb{N}_{(0,H-1)}$, the covariance at actuation time $a_{k,h}$ is given by

$$\Theta^a_{k,h} := \mathbb{E}[(x(a_{k,h}) - \hat{x}_{k,h})(x(a_{k,h}) - \hat{x}_{k,h})^\intercal \mid \mathrm{I}_k] = A(h^a)\Theta^a_{k,h-1}A(h^a)^\intercal + W(h^a), \tag{34}$$

where $\Theta^a_{k,0} := \Theta^a_k$ for all $k \in \mathbb{N}$. This multirate case is illustrated in Fig. 7.

Define $\bar{\Theta}^a_h$ as the solutions to (34) with $\Theta^a_{k,0} = \Theta^a$, with Θ^a as used in (27). For the multirate approach, the minimal value of (18) for $N \to \infty$ is given by

$$J^{MR} := \frac{1}{h^a}\tilde{c}_a, \quad \tilde{c}_a := tr(W(h^a)P + \tilde{\Theta}^a K^\intercal G K) + \alpha(h^a), \tag{35}$$

where $\tilde{\Theta}^a := \frac{1}{H}\sum_{h=0}^{H-1}\bar{\Theta}^a_h$ and where P, K, G are now computed from the smaller h^a.

Remark 4. A combination of switching and multirate is also possible. Such an approach would make the switching conditions more complex. Here, we focus on illustrating possibilities in image-based feedback instead of detailing all technicalities.

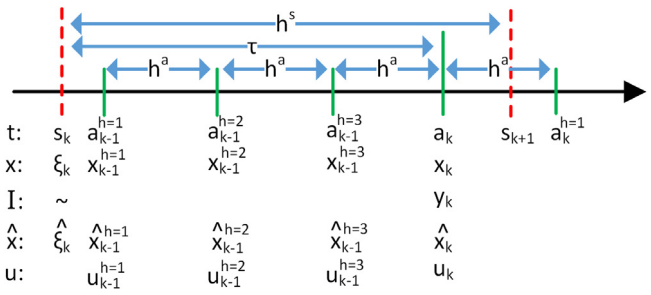

Fig. 7. Timings for small delay multirate control.

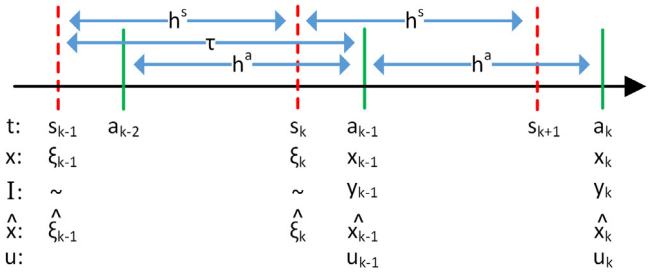

Fig. 8. Timings for large delay control.

5. Control design for $\tau > h^s$

For camera systems with variable imaging settings, the processing delay τ^p may be larger than one imaging interval τ^c. On the EM system that we consider, combining only two images to obtain a frame leads to the case when $\tau > h^s$, i.e., the total sensing-to-actuation delay τ may be larger than a sensing interval. Hence, we also present equations to compute controllers for this case, illustrating the differences. In particular, we focus on the case $2h^s > \tau > h^s$ from which extended cases (with larger differences between τ and h^s) may be derived by similar methods. The main differences with the small delay case $\tau < h^s$ are in the optimal estimator and result in a different state estimate. In fact, the actuation structure remains the same as for the small delay case and will not be explicitly discussed.

Recall that a shorter sampling interval typically results in less accurate information, hence a setup with shorter sensing interval does not necessarily lead to better performance, as we will show in Section 6. There is a clear trade-off here.

5.1. Single actuation instant

Fig. 8 depicts the case with $h^a = h^s$ with a large delay. At actuation time a_k, we compute the state estimate

$$\hat{x}_k = \mathbb{E}[x(a_k) \mid \mathrm{I}_k] = A(\tau)\xi_k + A(h^a)B(\tau - h^a)u_{k-2} + B(h^a)u_{k-1} \tag{36}$$

as a function of the last updated estimate of the state. The variance is computed by (21), but now with τ relatively larger than in Section 4.

The computation of ξ_k and Θ^s_k follows from (24) and (25), respectively. At time a_k, the previous prediction $\hat{\xi}_k$ is based on the previous estimate ξ_{k-1} that was updated based on the previous measurement y_{k-1}, as given by

$$\hat{\xi}_k = \mathbb{E}[\xi_k \mid \mathrm{I}_{k-1}] = \mathbb{E}[\mathbb{E}[x(s_k) \mid \mathrm{I}_k] \mid \mathrm{I}_{k-1}] = \mathbb{E}[x(s_k) \mid \mathrm{I}_{k-1}] = \mathbb{E}[A(h^s)x(s_{k-1}) + A(\tau - h^s)B(h^s - (\tau - h^s))u_{k-3} + B(\tau - h^s)u_{k-2} + w(s_{k-1}, h^s) \mid \mathrm{I}_{k-1}]$$

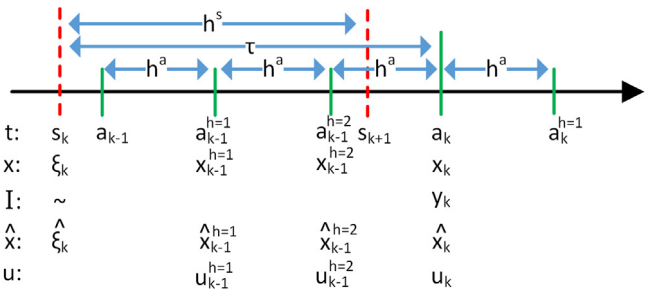

Fig. 9. Timings for large delay multirate control.

$$= A(h^s)\xi_{k-1} + A(\tau - h^s)B(2h^s - \tau)u_{k-3} + B(\tau - h^s)u_{k-2}.$$

The prediction made at time a_{k-1} will be used at time a_k. The corresponding covariance update is given by

$$\hat{\Theta}^s_k := \mathbb{E}[(x(s_k) - \hat{\xi}_k)(x(s_k) - \hat{\xi}_k)^\intercal \mid \mathrm{I}_{k-1}]$$
$$= A(h^s)\Theta^s_{k-1}A(h^s)^\intercal + W(h^s). \tag{37}$$

The stationary solution for the covariance estimates at actuation time can be found by computing the stationary solution to

$$\Theta^s_k = (I - L_kC)A(h^s)\Theta^s_{k-1}A(h^s)^\intercal(I - L_kC)^\intercal + (I - L_kC)W(h^s)(I - L_kC)^\intercal + L_kV_kL_k^\intercal \tag{38}$$

for Θ^s, with $L_k = \hat{\Theta}^s_kC^\intercal(C\hat{\Theta}^s_kC^\intercal + V_k)^{-1}$, and then inserting the solution in (21). Performance can then be computed using the same Eq. (27) as for the small delay case, but the actuation variance matrix is now relatively larger, in least-squares sense.

5.2. Multirate controller: faster actuation with large delay

Fig. 9 depicts the multirate case with a fractional actuation rate with a large delay. By using the solution to the single actuation results for the estimate at a_k with large delay, as given in the previous subsection, and the multirate approach for the subsequent actuation instants from the small delay case, as given in Section 4.5, again the optimal controller solution can be obtained. For conciseness, we omit the derivation of the equations.

6. Validation of control methodologies in a simulated industrial case study

To validate the proposed control designs, an electron microscope simulator with image-based feedback control is developed (in Matlab) based on the industrial expertise of Thermo Fisher Scientific, including several real-life ingredients. A minimal working example for the simulator framework, containing the main characteristics of the actual machines, is used to illustrate our methodologies. Other trackers and control designs can be implemented as well as other methods to generate the images (such as different blurring effects). In this section, we first present the details on the simulator implementation. Subsequently, we follow a work flow for the control design and implementation of the image-based feedback control system. Finally, we numerically validate the control designs using the simulator.

6.1. Simulator description

The simulator takes a large (high resolution) *benchmark image* and generates frames taking out a section from the benchmark image. We use a 4 k image source and generate frames

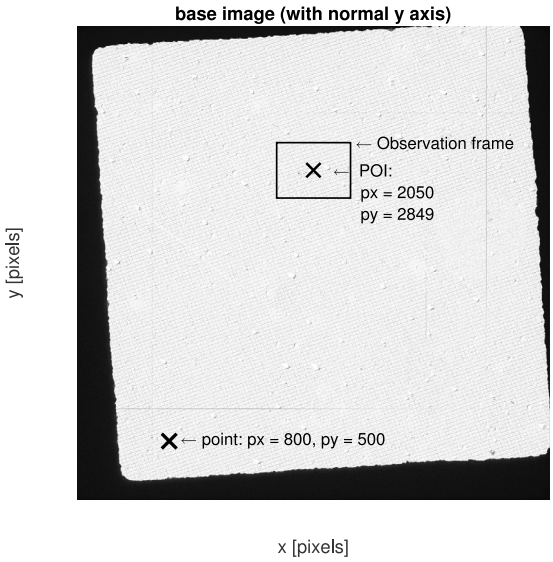

Fig. 10. 4k benchmark image of gold (Source image data courtesy of Thermo Fisher Scientific) with initial observation frame around the point of interest (POI).

of 640 × 480 pixels. The source image, which is obtained from industry, the POI and the initial observation frame that are used in this work are depicted in Fig. 10.

When frames are generated, the sections of the benchmark image are then first corrupted by Gaussian blurring, consistent with the total movement between frames, and then by Poisson noise, consistent with the electron arrival process, as explained in Section 2. The tracker uses the first frame to create a tracking template, which it searches for in the subsequent frames. We use a tracking template of 256 × 256 pixels. The tracker returns the expected position of the template in the frame, as detailed in Section 2.2. This position estimate is taken as input to a controller, which is designed according to Section 4 or Section 5, depending on the control configuration. In particular, a state estimate is computed and, subsequently, the control inputs are determined. Based on the chosen control inputs and randomly generated disturbances, the state is propagated according to the model (17). The new position of the state results in a change in the frame position with respect to the benchmark image. A new image is then generated, with blurring and noise, which closes the image-based feedback loop, see also Fig. 3. Linear interpolation is used to generate subpixel shift in the image.

The source image is normalized to have mean pixel intensity 1, which corresponds to an average of 1 counted electron per pixel and will later be multiplied by N^e. The velocity, induced by drift and stage actuation, is assumed to be approximately constant between samples. The total motion during image acquisition is determined by multiplying the velocity with the sensing interval h^s_k. The total movement in pixels is used as standard deviation for the Gaussian filter that generates blur. For a particular imaging session in electron microscopes, the doserate DR is a fixed constant. Hence, if N^i is fixed, N^e is also constant. To generate the frame with Poisson noise, the normalized frame values are multiplied by the chosen value of N^e such that the average intensity is approximately N^e as explained in Section 2.2. The resulting pixel values are used as the parameter for Poisson distributions. This generates images that are accurate representatives of those of a real EM system.

Note that, in this work, we assume the POI to be within the observation frame at all times since the loss of the POI is not taken into account in the current control design framework.

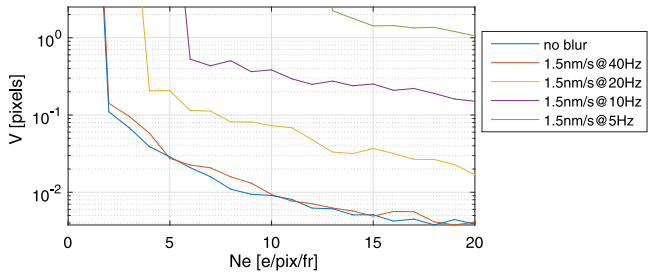

Fig. 11. Measurement inaccuracy V versus N^e (logarithmic). Increased N^e improves accuracy. The impact of blur is less when sampling faster.

Furthermore, we do not consider the case where the POI is identified in the wrong location. Adaptive methods to deal with such cases may be combined with the approaches proposed here, but this is beyond the scope of this paper.

In the remainder of this section, we explain the steps taken to identify the relevant system parameters and provide numerical results to illustrate and validate the control designs presented in this paper.

6.2. Work flow for design and implementation

To implement the proposed control solutions and validate them in this simulation environment, several steps are required. The steps taken in this work can be summarized as follows.

(1) Identify appropriate disturbance parameters d_0^v and B_{w^d}.
   (a) Choose the values based on suggestions by industrial experts inferred from experience.

(2) Identify the measurement accuracy V_k for several system settings.
   (a) Generate open-loop images and analyze the tracking error to estimate the variance.

(3) Compute controller variables (K and L) and expected performance (J) for several system settings.
   (a) Compare in theory and validate in (simulated) experiments.

(4) Compute and validate advanced controllers.
   (a) Compare in theory and validate in (simulated) experiments.

Next, we illustrate these steps numerically.

Note that d_0^v is only required for simulation purposes and that in the implementation it will be estimated by the Kalman filter. In practice, as a general problem for LQG-type control designs, it may be difficult to choose a good estimate for B_{w^d} and online learning methods are often employed to improve upon the initial choice of parameter. The same holds for the measurement noise V.

6.3. Disturbance and cost parameters

Based on suggestions by industrial experts, an appropriate choice for the initial drift is $d_0^v = 1.5$ nm/s, which eventually causes the object to leave the FOV if uncontrolled. Note that d_0^v is not available to the observer and the initial drift estimate is equal to 0.

We select $B_{w^d} = 1$ nm/s to create variations in the drift and we assume no other disturbance source, hence we take $B_{w^e} =$ 0 nm. In a real-life setting, B_{w^d} should be estimated, e.g., by an online method or by an open-loop identification procedure (see, e.g., Odelson, Rajamani, & Rawlings, 2006).

The cost is chosen as $Q_e = 1$ and $R_u = 0.01$ such that there is only a small penalty on actuation.

6.4. System settings and measurement accuracy

We consider a system with a maximum camera rate of $f_c = 40$ Hz corresponding to a minimal acquisition interval of $\tau^c = 25$ ms. The doserate of the exposure is $DR = 50$ e/pix/s. This corresponds to $N^e_{min} = 1.25$ e/pix/frame. The resolution of the camera is $r = 0.1$ nm/pixel.

We consider a tracker with a processing delay of $\tau^p = 29$ ms. The requirement $\tau < h^s$ such that $a_k \leq s_{k+1}$ requires $N^i \geq 3$. For $N^i = 3$, $\tau = 66.5$ ms and $h^s = 75$ ms. As already mentioned, the tracker is the single-step DFT algorithm (Guizar-Sicairos et al., 2008), which implements a normalized cross-correlation filter with approximated subpixel accuracy of $\frac{1}{100}$th of a pixel.

The image quality depends on N^e, which determines the level of Poisson noise, and on the motion blur. Note that the accuracy of the measurements typically also depends on the contrast in the content of the image itself, the study of which is out of the scope of this work. We first compute randomly perturbed sequences of images for variations in N^e without any blur. This corresponds to an optimal measurement situation and gives a baseline for the accuracy of the tracker as a function of N^e. We also compute sequences with a motion blur consistent with a constant drift of 1.5 nm/s at imaging rates of 5, 10, 20 and 40 Hz. At least 500 images were used in each sequence. Fig. 11 illustrates that the blur can significantly impact the accuracy. For $N^i < 3$, which would result in the case in Section 5, we see that the image quality is very low and misidentifications of the tracker occur. Hence, we do not analyze these cases here. This also occurs for higher N^i if much motion blur is present, as can be seen in Fig. 11 by the steep increase of the accuracy curves. Autocorrelation and the histogram of the measurement noise were computed and supported the assumptions of independence and Gaussianity.

Recall that $N^e = N^e_{min} \times N^i$ and that N^i is directly related to h^s, such that Fig. 11 also represents a relation between the sensing interval and the accuracy.

The above parameters are used in the control designs proposed in this paper.

6.5. Two-phase control and processing approach

We consider two phases in the behavior of the closed-loop system. In the first phase, the main drift velocity is not yet compensated by the stage motion and the POI moves away from the imaging center. The main objective in this phase is to obtain a good drift estimate and stabilize the POI near the imaging center by actuating the stage. Once the main drift component is appropriately counteracted, the motion blur will reduce and image quality will improve. In the second phase, the main controller goal is to minimize the position error such that the POI is at or near the center of the frame. To this end, the tracking template may be updated to improve measurement accuracy. Furthermore, a controller for higher measurement accuracy may be selected at that time as well. Here, we illustrate the two control phases separately, while in practice online updating of the template, e.g., by a recursive filter, can be implemented to make the transition more gradual from a sensing perspective. Next, we numerically illustrate these two phases separately to ease the analysis.

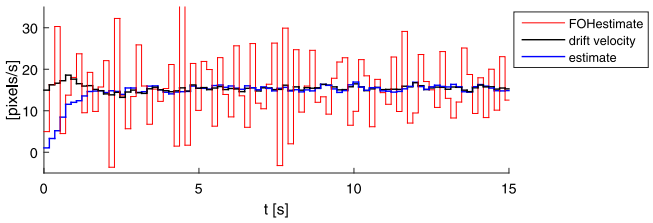

Fig. 12. Comparison of the actual drift velocity to the drift estimates based on the measurements between the proposed observer of the control algorithm, i.e. (20) or (36), and to a first-order hold (FOH) estimate.

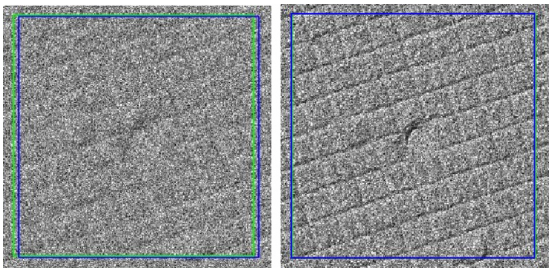

Fig. 13. Part of frames with initial blur (left) and with low blur after correction of the main drift component (right). Blur causes significant accuracy problems in the tracker, i.e., an error between the measured position (blue square) and the true area around the POI (green). (For interpretation of the references to color in this figure legend, the reader is referred to the web version of this article.)

6.5.1. Phase 1: Drift velocity estimation and stabilization

Here, we assume that a low-quality template has been obtained, which has been corrupted by a significant amount of motion blur. Since the effect of the blur is difficult to quantify, a non-switched LQG-type controller is implemented and its performance studied. As Fig. 12 illustrates, it takes several measurements over several seconds (approximately 2 s) for the observer to obtain a reasonably accurate estimate of the drift velocity. Clearly, the observer estimate is much better than a first-order hold estimate based on the measurements directly, provided that measurement and noise parameters are accurately identified. Since estimation and subsequent compensation of the drift only takes several seconds, this first phase can already significantly increase throughput of the overall system. The difference in blur before and after compensation is depicted in Fig. 13. Clearly, updating the template will improve accuracy, as even small tracking errors can cause significant imaging aberrations.

6.5.2. Phase 2: Improved stabilization

In this second phase, we assume a high-quality template has been obtained and the blurring effect is small. Then, the measurement variance can be assumed small, e.g., we can assume a best-case scenario (which is what we aim to achieve) and let the variance only depend on N^e. In particular, we assume that there is no blurring and compute the variance V for $N^e = 1, \ldots, 30$ using 1000 open-loop images. The relation between the variance and the number of electrons is depicted in Fig. 14.

Fig. 15 depicts the theoretical control performance (27) for variations in h^s, corresponding to $3 \leq N^i \leq 30$, for $B_{w^d} = 1$. Fig. 15 clearly illustrates how the trade-off between delay and accuracy, as illustrated by Fig. 14, results in variations of performance for the EM system considered in this work. Settings and cost corresponding to different N^i are given in Table 1. For the chosen system settings, the best performance for the LQG-type control without switching is obtained by selecting $N^i = 5$. The cost seems to increase for $N^i < 3$, therefore not considering those cases is validated. If B_{w^d} is smaller, the curve in Fig. 15 dips more on the right side and the optimum shifts right.

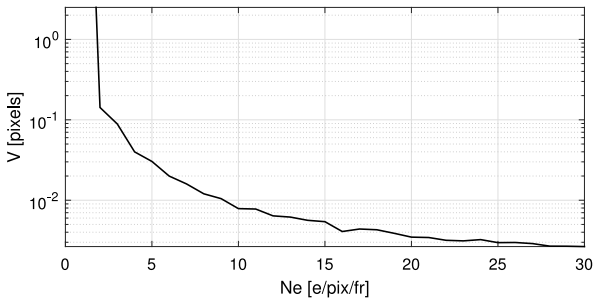

Fig. 14. Measurement inaccuracy V versus N^e (logarithmic) without blurring effect based on generated experimental images.

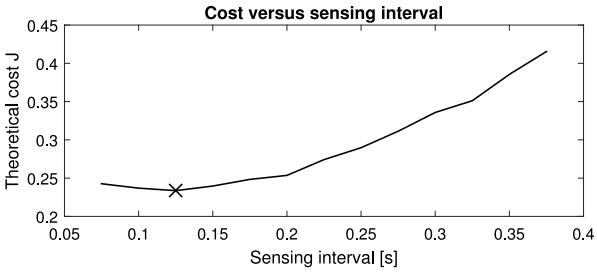

Fig. 15. Control performance J versus h^s ($N^i \geq 3$), optimum indicated by $\times$.

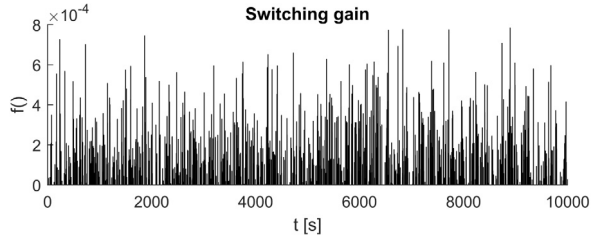

Fig. 16. Switching gain for one Monte-Carlo experiment.

Table 1
For computational reasons and because the optimum is expected at $N^i = 5$, not all values for J^{sim} and J^{exp} were computed.

N^i	h^s	τ	N^e	V	J^{theory}	J^{sim}	J^{exp}
3	0.075	0.0665	3.75	0.0522	0.2426	0.2430	
4	0.100	0.0790	5	0.0304	0.2369	0.2372	0.2405
5	0.125	0.0915	6.25	0.0190	0.2336[a]	0.2339	0.2366
6	0.150	0.1040	7.50	0.0140	0.2396	0.2401	
7	0.175	0.1165	8.75	0.0109	0.2483		
8	0.200	0.1290	10	0.0079	0.2536		

[a]Performance for several system settings with best setting.

To verify the theoretical results, we perform Monte-Carlo (MC) simulations in which the disturbances are randomly generated. First, MC simulation without actual images were performed to verify the theoretical expected cost for $3 \leq N^i \leq 6$. The measurement noise was randomly generated with corresponding variance V. Simulation time was 10 000 s, such that the average cost, given in Table 1, had approximately converged, for 50 MC simulations.

From the non-switched results, we find that $b^\star$ is given by the mode with $N^i = 5$ and we can compute switching conditions as given in Section 4.4. We perform a simulation with switching

and obtain a cost of $J^{sim}_{switched} = 0.2339$, which is equal to the best non-switching cost $J^{sim}_{b^\star} = 0.2339$ found for $N^i = 5$.

Nevertheless, we observed frequent switching between modes $N^i = 4$ and $N^i = 5$ (the other modes were not used). This illustrates that the switched controller guarantees equal performance to the non-switched case as expected from van Horssen et al. (2019). Next, experiments using the simulator will illustrate potential performance improvement due to the impact of control on the image quality.

We select modes $N^i = 4, 5$ for experimental simulation (experiments) with images and switching. Note that we restrict the number of modes for simulated experiments since the current implementation is a proof-of-concept that is not computationally efficient and requires significant amounts of time when the simulation time is large, even when the number of MC simulations is small. Hence, we perform experiments for 10 000 s, such that the average cost had approximately converged, for 12 MC simulations.

The non-switching controllers perform slightly worse than expected ($J^{sim}_4 = 0.2372, J^{sim}_5 = 0.2339$ and $J^{exp}_4 = 0.2405, J^{exp}_5 = 0.2366$), which can be attributed to the blurring effect that was not taken into account in the pure simulations or when the values of V in Table 1 where determined. Initially, we use the switched controller with switching conditions based on the best case parameter for V, as given in Table 1, and we obtain $J^{exp}_{switched, V_{bestcase}} = 0.2388$, which is not an improvement over both methods due to the fact that the switching expects a better cost when switching than can be realized. To correct for the mismatch between the cost for expected V and the realized cost, we correct the expected cost by recomputing the estimation variables, especially a new solution to (26), for a new V_{true}. Note that, for fair comparison, we kept all observer gains equal to those computed for the original $V_{bestcase}$. We find that for a small adjustment to $V_{true} = 0.0320, 0.0199$, for $N^i = 4, 5$, amount to a theoretical cost (27) equal to the values found for J^{exp}_4, J^{exp}_5, respectively. After this correction for the cost predictions, the switched controller performs slightly better than both non-switched controllers at a cost $J^{exp}_{switched} = 0.2362$, although the improvement is very small (order of 0.2%). As expected, a good model is required to make a good cost prediction and to realize appropriate switching to improve performance. In Fig. 17, the position, the position estimate and the measurement are depicted, illustrating how the observer improves the estimation error by filtering the variations in the measurements. Consistent switching at random instants is observed in the MC simulations and experiments. The expected switching gain, i.e., the predicted cost differences in (28) with the choice $b^\star$, for one experiment is depicted in Fig. 16. The expected gain per switch is small, but over time a performance improvement is achieved. The gain depends on many factors such as the system itself but also the available system settings. The results motivate further study as to which system settings should be used for control and for switching.

The current results show feasibility of the switched approach. Here, a switching horizon of one step was selected. Based on van Horssen et al. (2019), switching conditions for a larger horizon can be derived which may increase the expected switching gains. One simulation shows that, even without initial drift, in 500s the random walk due to B_{w^d} could have caused a position drift of 5000 pixels if the system was uncontrolled. Hence, the relevance and importance of closed-loop image-based feedback are clear.

6.5.3. Multirate performance

For comparison, we analyzed the theoretical performance of the system for different multirate settings, described in Section 4.5. The relation between the number of update instants

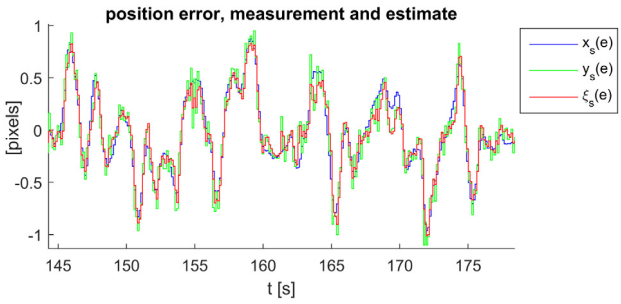

Fig. 17. Error, measurement and estimate.

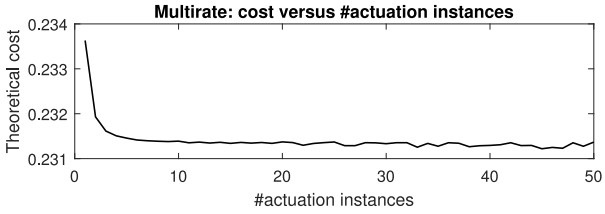

Fig. 18. Multirate performance J versus the number of actuation instants between samples for mode $N^i = 5$.

and the expected cost is depicted in Fig. 18 for $N^i = 5$. We observe that the control performance improves monotonically up to approximately 0.2313 (1.1% improvement compared to one actuation instant) but the gain by updating faster is limited after using more than ten actuation instants per measurement. Hence, we can expect that increasing the control rate will improve performance provided that an accurate model is available. Note that for large numbers of actuation instants the discretization of the cost variables can become numerically difficult due to h^a being small, which can lead to numerical problems in computation of the cost, as can be seen in Fig. 18 for more than 20 update instants by the non-monotonic decrease.

7. Conclusion

This paper demonstrated how an image-based feedback control loop can be designed for active drift compensation in an electron microscope, where the required measurements (regarding drift) can be only obtained through the images themselves. We illustrated how drift, which is partly random, can be counteracted by the movement of the specimen that is in view by using only information extracted from images. Our solution was based on a stochastic model for the drift, which was proposed based on insights from industrial experts. An LQG-type control design was proposed, which was shown to achieve automatic stabilization of the image, and can thereby improve image quality and throughput considerably. This was validated on a relevant industrial case study using a simulator for feedback control based on images that are generated online in a closed-loop structure. This simulator was developed based on discussions with industrial experts and uses real trackers and images from the EM industry. The trade-off between measurement accuracy and sensing delay has been shown using industry-proposed parameters for the sensing system, which involves a data-acquisition delay consisting of both image-acquisition delay and image-processing delay. Variations on the model-based control design methods are proposed to improve image quality further. In particular, feasibility of the novel switched controller design approach proposed in van Horssen

et al. (2019) is demonstrated, which can exploit flexibility in data acquisition to improve performance. While the results for the current set-up are not improved much by switching, it provides a solid basis for the redesign of the hardware and software components of the imaging system of the industrial partner.

Several directions for further study are of interest. (i) The simulator can be equipped with different trackers, other source images, or other motion blur filters. Rotations of the image may be accounted for in the image-processing step by the tracker, but nonlinear control approaches can also be studied. (ii) Implementation of the methods on a real system is, of course, another important recommendation for future work. To make the framework more robust, possible failure of the feature tracker should be addressed in either the tracker, an adaptation of the controller and/or another safety system. (iii) For truly SISO systems, loopshaping control designs may be more intuitive to some designers than the state–space design approach taken here, hence studying the relation between loopshaping parameters and the LQG-type tuning parameters can provide new insights. Here, a LQG-type approach was taken for the ease of extension to a MIMO solution, corresponding to the two-dimensional nature of the images. A comparative analysis to PID-type or other types of controllers would be valuable, although an analogy for the MIMO and switching nature of the proposed methods requires further study. The simulation environment allows the implementation of other types of controllers. (iv) Currently, experimentation using the simulator takes a significant amount of time if many Monte-Carlo runs or long experimentation times are desired. Optimization of the implementation of the simulator can reduce experimentation times, e.g., by parallelization or implementation in dedicated hardware. (v) Methods such as Odelson et al. (2006) may be helpful in (online) estimation of variances, such that open-loop experiments are not needed. Analysis of more benchmark images will give a better understanding of variations in the relation between measurement variance and contrast in the image content. (vi) An implementation with a time-varying Kalman filter may improve performance as discussed in Remark 2. (vii) If a fast beam-steering mechanism is in place, the proposed engineering framework can be applied to correct for drift by beam-steering. This could be an interesting alternative for, e.g., scanning-type microscopes, but may require more complex low-level controllers. (viii) Also, a combined switching multirate design is an interesting subject for study.

As a final comment, this paper laid down a design framework that demonstrates the potential of (switched and non-switched) feedback controllers for drift compensation in EMs leading to significantly improved imaging (compared to the uncontrolled case) at high throughput. The framework offers many directions for further research and as such is an important starting point for further studies in this relevant application domain.

Declaration of competing interest

The authors declare that they have no known competing financial interests or personal relationships that could have appeared to influence the work reported in this paper.

CRediT authorship contribution statement

E.P. van Horssen: Conceptualization, Methodology, Software, Formal analysis, Investigation, Writing - original draft. **B.J. Janssen:** Supervision, Resources, Writing - review & editing. **A. Kumar:** Investigation, Software. **D. Antunes:** Supervision, Methodology. **W.P.M.H. Heemels:** Supervision, Methodology, Writing - review & editing.

References

Andersson, S. B., & Abramovitch, D. Y. (2007). A survey of non-raster scan methods with application to atomic force microscopy. In *American control conference* (pp. 3516–3521). IEEE.

Andersson, S. B., & Park, J. (2005). Tip steering for fast imaging in AFM. In *Proceedings of the 2005, American control conference, 2005. Vol. 4* (pp. 2469–2474).

Åström, K. J. (1970). *Introduction to stochastic control theory*. Elsevier.

Åström, K. J., & Wittenmark, B. (2013). *Computer-controlled systems: Theory and design*. Courier Corporation.

Bar-Shalom, Y., & Li, X.-R. (2001). *Estimation with applications to tracking and navigation*. New York, NY, USA: John Wiley & Sons, Inc..

Bertsekas, D. P. (2005). *Dynamic programming and optimal control, Vol. 1 and Vol. 2* (3rd ed.). Athena Scientific.

Chen, T., & Francis, B. (1995). *Optimal sampled-data control systems*. Springer-Verlag.

Colaneri, P., & de Nicolao, G. (1995). Multirate LQG control of continuous-time stochastic systems. *Automatica*, *31*(4), 591–596.

Colaneri, P., Scattolini, R., & Schiavoni, N. (1990). Stabilization of multirate sampled-data linear systems. *Automatica*, *26*(2), 377–380.

Corke, P. (2011). *ser. Springer tracts in advanced robotics, Robotics, vision and control - fundamental algorithms in MATLAB* (p. 73). Springer.

Doornbos, R., & van Loo, S. (2012). *From scientific instrument to industrial machine: Coping with architectural stress in embedded systems*. Springer Publishing Company, Incorporated.

Egerton, R. F. (2005). *Physical principles of electron microscopy*. Springer.

Elmokadem, A., & Yu, J. (2015). Optimal drift correction for superresolution localization microscopy with bayesian inference. *Biophysical Journal*, *109*(9), 1772–1780.

FEI (2010). https://www.fei.com/documents/introduction-to-microscopy-document/ (accessed 30-10-2017).

Geromel, J. C., Deaecto, G. S., & Daafouz, J. (2013). Suboptimal switching control consistency analysis for switched linear systems. *IEEE Transactions on Automatic Control*, *58*(7), 1857–1861.

Gonzalez, R. C., & Woods, R. E. (2006). *Digital image processing* (3rd ed.). Upper Saddle River, NJ, USA: Prentice-Hall, Inc..

Guizar-Sicairos, M., Thurman, S. T., & Fienup, J. R. (2008). Efficient subpixel image registration algorithms. *Optics Letters*, *33*(2), 156–158.

van Horssen, E. P., Antunes, D., & Heemels, W. P. M. H. (2015). Switching data-processing methods for feedback control: Breaking the speed versus accuracy trade-off. In *Decision and control (CDC), 2015 IEEE 54th annual conference on* (pp. 2313–2318).

van Horssen, E. P., Antunes, D., & Heemels, W. P. M. H. (2019). Switched lqg control for linear systems with multiple sensing methods. *Automatica*, *103*, 217–229.

Jin, P., & Li, X. (2015). Correction of image drift and distortion in a scanning electron microscopy. *Journal of Microscopy*, *260*(3), 268–280.

Krautgartner, P., & Vincze, M. (1998). Performance evaluation of vision-based control tasks. In *Proceedings. 1998 IEEE International Conference on Robotics and Automation, Vol. 3* (pp. 2315–2320).

Odelson, B. J., Rajamani, M. R., & Rawlings, J. B. (2006). A new autocovariance least-squares method for estimating noise covariances. *Automatica*, *42*, 303–308.

O'Keefe, M., Parvin, B., Owen, D., Taylor, J., Westmacott, K., Johnston, W., et al. (1996). Automation for on-line remote-control in situ electron microscopy. In *Proceedings of the fifteenth pfefferkorn conference*.

Reimer, L., & Kohl, H. (2008). *ser. Springer series in optical sciences, Transmission electron microscopy: Physics of image formation*. New York: Springer.

Salmons, B. S., Katz, D. R., & Trawick, M. L. (2010). Correction of distortion due to thermal drift in scanning probe microscopy. *Ultramicroscopy*, *110*(4), 339–349.

Se, S., Lowe, D. G., & Little, J. J. (2005). Vision-based global localization and mapping for mobile robots. *IEEE Transactions on Robotics*, *21*(3), 364–375.

Sharkey, P. M., & Murray, D. W. (1996). Delays versus performance of visually guided systems. *IEE Proceedings D (Control Theory and Applications)*, *143*(5), 436–447.

Sutton, M., Orteu, J., & Schreier, H. (2009). *Image correlation for shape, motion and deformation measurements: Basic concepts, theory and applications*. US: Springer.

Tarău, A. N., Nuij, P., & Steinbuch, M. (2011). Hierarchical control for drift correction in transmission electron microscopes. In *2011 IEEE international conference on control applications (CCA)* (pp. 351–356).

Zhang, L., Long, Q., Liu, Y., Zhang, J., & Feng, Z. (2016). Correlation-steered scanning for scanning probe microscopes to overcome thermal drift for ultra-long time scanning. *Ultramicroscopy*, *166*(Supplement C), 16–26.

Eelco P. van Horssen received the M.Sc. degree (cum laude) in electrical engineering in 2013 from the Eindhoven University of Technology (TU/e), Eindhoven, The Netherlands. In 2018, he obtained the Ph.D. degree from the department of mechanical engineering of TU/e on the topic of "Data-intensive feedback control: switched systems analysis and design".

He is currently a dynamics, systems, and control engineer in industry.

Bart Janssen received the M.Sc. degree in electrical engineering and the Ph.D. degree in mathematical image analysis both from the Eindhoven University of Technology (TU/e), Eindhoven, The Netherlands.

Since 2011 he has been working on electron microscopes for FEI, and later Thermo Fisher Scientific. His research interests include images sensors for electron detection, and image-based control.

Ayush Kumar was born on 26 February, 1992 in India. He has a bachelors degree from VIT University, Vellore, India in Electronics and Instrumentation Engineering. He moved to the Netherlands in 2015 and in 2017 obtained the M.Sc. degree in Systems and Control from the Eindhoven University of Technology (TU/e), Eindhoven, The Netherlands.

He worked as Control Engineer in a logistic automation company Vanderlande, Veghel, The Netherlands for two years. Presently, he is working as systems engineer in Rovisys, Utrecht, The Netherlands.

Duarte Antunes was born in Viseu, Portugal. He received the Licenciatura in Electrical and Computer Engineering from the Instituto Superior Técnico (IST), Lisbon, in 2005. He did his PhD (cum laude) from 2006 to 2011 in the research field of Automatic Control at the Institute for Systems and Robotics, IST, Lisbon, in close collaboration with the University of California, Santa Barbara.

From 2011 to 2013 he held a postdoctoral position at the Eindhoven University of Technology (TU/e). He is currently an Assistant Professor at the Department of Mechanical Engineering of TU/e.

His research interests include networked control systems, stochastic control, approximate dynamic programming, and robotics.

W.P.M.H. (Maurice) Heemels received the M.Sc. degree in mathematics and the Ph.D. degree in control theory (both summa cum laude) from the Eindhoven University of Technology (TU/e), the Netherlands, in 1995 and 1999, respectively. From 2000 to 2004, he was with the Electrical Engineering Department, TU/e, as an assistant professor, and from 2004 to 2006 with the Embedded Systems Institute (ESI) as a research fellow. Since 2006, he has been with the Department of Mechanical Engineering, TU/e, where he is currently a Full Professor. He held visiting professor positions at the Swiss Federal Institute of Technology (ETH), Switzerland (2001) and at the University of California at Santa Barbara (2008). In 2004, he worked also at the company Océ, the Netherlands.

His current research interests include hybrid and cyber–physical systems, networked and event-triggered control systems and constrained systems including model predictive control.

Dr. Heemels served/s on the editorial boards of *Automatica*, *Nonlinear Analysis: Hybrid Systems*, *Annual Reviews in Control*, and *IEEE Transactions on Automatic Control*. He was a recipient of a personal VICI grant awarded by STW (Dutch Technology Foundation). He is a Fellow of the IEEE. He is currently chair of the IFAC Technical Committee on Networked Systems.